9B.3 Monitoring the data quality of the new polarimetric weather radar network of the German Meteorological Service

Michael Frech*, Deutscher Wetterdienst
Hohenpeissenberg Meteorological Observatory, Germany

1. Introduction

The German Meteorological Service DWD is currently replacing all radar systems with new dualpolarization radars. With the introduction of dualpolarization systems improved quantitative precipitation estimations and a better classification of meteorological and non-meteorological targets are expected. Along with the radar hardware replacement the project "Radarmassnahmen" has been launched to develop a centralized data processing chain for the dualpol data and subsequent products. The radar processing chain "POLARA" consists of a data quality assurance module, a fuzzy logic hydrometeor classification scheme (HMC) and a quantitative precipitation estimate (QPE) module. An important component of this project is the development of operational data quality monitoring methods including the verification and monitoring of dualpol data quality. Here we focus on the data quality that can be affected by the radar hardware, in particular on the receive and transmit path of the radar signal. Further quality checks and an attenuation correction are implemented in the centralized data processing chain (Tracksdorf et. al. 2013, Steinert et al., 2013).

It is well known that dualpol moments must satisfy requirements with respect to accuracy and uncertainty before the full benefit for QPE and HMC can be seen. The key moments we consider are the horizontal reflectivity factor Zh, the differential reflectivity ZDR, the cross correlation coefficient ρ_{hv}, the differential phase Φ_{dp}, and based on latter moment, the specific differential phase K_{dp}. The accuracy of those moments is affected by various aspects. The sampling strategy to compute the moments has a strong influence on the resulting accuracies (Melnikov, 2004). Therefore the scan strategy must consider the requirements to obtain good radar data quality from a scanning radar (Seltmann et al, 2013). The effect of the radar hardware on the dualpol moments also has to be considered. Since we use the simultaneous transmit and receive mode we have to make sure that the analog signal path from transmit to receive is well characterized and monitored for the horizontal and vertical polarization state. The goal is to achieve an accuracy better than 1 dB in Z and 0.1 dB in ZDR. An important element here is the antenna (Frech et al., 2013). The antenna characteristics in H and V must match very well not only during the acceptance of a system but also during the lifetime of the radar system. For example the feed could defocus which may result into increased side-lobe levels and increased beam-squint. This in turn would affect the clutter suppression performance and the interpretation of differential reflectivity in areas with large reflectivity gradients. So monitoring the transmit and receive path is an important aspect of the overall data quality monitoring. Up to now the following aspects are considered in our monitoring scheme at the radar site:

- monitoring the absolute calibration: using measurements of a birdbath scan at 90° elevation and disdrometer measurements at the radar sites.
- system differential offsets of ZDR and Φ_{dp}: using measurements of an operational birdbath scan at 90° and the detected solar signals in the operational scanning.

*Corresponding author address: Michael Frech, DWD, Meteorologisches Observatorium Hohenpeissenberg, D-82383 Hohenpeissenberg, Germany. Email: Michael.Frech@dwd.de
Extented abstract, AMS Radar conference 2013, Breckenridge, CO, USA.

- analysis of solar signals from the operational scanning: monitoring the receiver sensitivity ($dBm0_{h,v}$), differential offset of the receive path (ZDR), antenna pointing accuracy, beam squint.

Our experience shows that the aging of the hardware is often visible as more or less weak, sometimes transient trends. Making those trends visible is an important aspect which can be used to initiate preventive maintenance actions well in advance of a possible hardware failure or a failure of radar data based algorithms (i.e. a hydrometeor classification) which may be affected by degraded radar data quality. This is an important aspect as it guarantees a high availability of the radar systems. The continuous monitoring of the radar systems is even more important in light of the fact, that the maintenance interval is extended to 9 months.

In this contribution we first show results long term operational radar data monitoring using sun interferences (sun rays) during the operational scanning based on 9 new radar systems (see Holleman and Beekhuis (2004), Huuskonen and Holleman (2007), Figuras et al., 2013; see also the first results presented in Tabary et al., 2009).

Then we introduce and discuss the monitoring of the absolute calibration using the Thies optical disdrometer (PWS, present weather sensor). Currently 3 PWS are installed so that we only show results from three radar systems: Offenthal (OFT; near Frankfurt) , Boostedt (BOO; North of Hamburg, maritime environment) and Hohenpeissenberg (MOHP, South of Munich, close to the Alps, situated 1000 m above sea level). We then show the results of the monitoring of ZDR and Φ_{dp} offsets based on the birdbath scan and the analysis of solar interferences by the radar during operational scanning.

We conclude with a summary and an outlook on further developments.

2. The DWD radar network

The German Meteorological Service DWD is operating the national radar network. The network consists of 17 C-Band radar systems which cover most of the German territory. An additional system serves as a research radar which is operated at the Hohenpeissenberg Observatory. There, new technologies, radar data processing algorithms, radar software and new products are developed, tested and evaluated before they are introduced into operational service. Within DWD's radar system replacement project RadSys-E, all radar systems are replaced. The old radar systems are replaced with EEC's Doppler weather radar DWSR5001C/SDP/CE which has polarization diversity (SDP, simultaneous dual polarization). The complete replacement of all radar systems is scheduled to be finished in 2014. In the end, the operational network will consist of 17 operational radars and one research radar.

Here we summarize briefly some key aspects of the radar system:

Pedestal unit: pointing accuracy $< 0.05°$, maximum azimuth rate 48 °/s

Transmitter: Magnetron based transmitter, peak power 500 kW (so 250 kW for the H and V channel each). Frequency range 5600 to 5650 MHz. Four pulse widths: 0.4, 0.8, 2 and 3 μs.

Receiver: The receiver is mounted behind the antenna ("receiver-over-elevation" concept). The analog signals are digitized by the ENIGMA3p IFD and the digitized IQ-data are transmitted in realtime through a fiber optic rotary joint to the ENIGMA3p signal processor which is mounted in the radar control cabinet. The dynamic range of the dual IF receiver is $\geq$ 105 dB.

Signal processor: Linux based signalprocessor ENIGMA3p

Antenna: The parabolic antenna has a diameter of 4.3 m and consists of 9 elements. The dish is made of a composite material and has a center-fed antenna design with four struts supporting the dualpol feed.

Radome: AFC radome 20DSF17 with a quasi random panel design which is optimized for dualpol applications. The panels have a sandwich foam core design. The radome is coated with a highly hydrophobic material and has a diameter of 6 m.

In the operational scanning we use two pulse widths, 0.4 and 0.8 μs. For this, the manufacturers calibration procedure requires four independent calibrations: 0.4 μs

in H & V, and 0.8 μs in H & V. It is clear that differential offsets will change every time a new calibration is performed. This due to the inherent uncertainty of the method. Currently the calibration data of the system is not changed if the new values are within 0.5 dB with respect to the current calibration data.

3. Methodology to estimate the solar power from radar measurements

The solar flux measurements are available daily (2-3 times) from the Dominion Radio Astrophysical Observatory (DRAO) in Canada. It is a solar flux measurement monitored at $\lambda = 10.7cm$ (S-Band). This is the independent flux measurement which is used to monitor the absolute receiver sensitivity of the radar system. In a first step the S-Band solar flux has to be converted the corresponding C-Band flux. Parameterizations of solar C-Band flux as a function of the S-Band flux are documented in literature (Tapping 2001).

$$F_C = 0.71 \cdot (F_{10.7} - 64) + 126 \tag{1}$$

with $F_{10.7}$, the adjusted solar flux (in sfu, solar flux unit) from DRAO (a sfu has units of $10^{-22}\frac{W}{m^2 Hz}$)

The maximum received solar power the radar system may measure needs to take into account the receiver bandwidth Δf and the effective antenna area A. For the C-Band system at Hohenpeissenberg $\Delta f \approx 1.38MHz$ with pulse length 0.8μs and $\Delta f \approx 2.61MHz$ for 0.4 μs, and $A = 13.85$ m^2. Then, the received solar power p_{sun} in mW is:

$$p_{sun} = \frac{1}{2} \cdot 10^{-13} \cdot \Delta f \cdot A \cdot F_C \tag{2}$$

A factor of 0.5 is introduced since the solar flux is an un-polarized source whereas the radar system is sensitive to horizontal or vertical polarization only. The solar power p_{sun} is compared to the actual power measurements from "sun rays" extracted from the operational data volumes. The implementation adopted and extended based on Holleman and Beekhuis (2004). Rays with a solar signal are solely detected by the time stamp of the ray. Based on this time stamp the solar position is computed and the ray with a solar signal is detected. For our scan strategy, about 30 rays with a solar signal are found in the operational data per day, depending on the season.

Instead of recalculating the received solar power from the radar reflectivity factor Z we directly employ the measured SNR to compute the received solar power. The signal-to-noise ratios from the horizontal (SNRh) and vertical (SNRv) receiver channels are operationally available as standard moments. The advantage of using SNR is that we can easily compute the received power knowing dBm0 which is determined during calibration. The value of dBm0 is defined as the interception point of the noise floor with the linear receiver response curve. The signal-to-noise ratio is $SNR = 0$ dB at this interception point. So it is straight forward to compute the received power $P_{h,v}$ using the measured SNR values together with dBm0:

$$P_{h,v} \quad = \quad SNR_{h,v} + dBm0_{h,v} \tag{3}$$

Since we want to relate $P_{h,v}$ to the received solar power we need to correct for the one-way gas attenuation A_{gas} of the sun power due to the Earth's atmosphere. This is estimated using a 4/3 Earth's radius model where the ray path r up to the top of the atmosphere is approximated using a standard atmosphere:

$$r(z, el) = R_{43}\sqrt{\sin^2 el + \frac{2z}{R_{43}} + \frac{z^2}{R_{43}^2}} - R_{43}\sin el \tag{4}$$

The gaseous attenuation can be approximated as:

$$A_{gas}(el) \approx a \cdot r(z_0, el) \tag{5}$$

with z_0, the equivalent height of a homogeneous atmosphere. A homogeneous atmosphere is defined by constant air density with height. Using typical values of a standard atmosphere, the height of a homogeneous atmosphere is $z_0 \approx 8.4km$. For a we assume $a = 0.008dB/km$.

We use a simple refraction correction which is optionally available as part of the implemented perl routines (Saemundsson, 1986). The effect of refraction depends on atmospheric conditions (pressure, temperature, relative humidity) and on the wavelength. For mean conditions ($p = 1010$ hPa, T $= 10°$C, yellow light) the refraction R can be written as:

$$R = \frac{1.02}{\tan\left(el_t + \frac{10.3}{el_t + 5.11}\right)}. \quad (6)$$

R has units of minutes of arc. el_t is the true sun elevation without an atmosphere. The apparent (observed) sun elevation is $el_a = el_t + R$.

So the attenuation corrected received solar power can be written as

$$P_{h,v} = SNR_{h,v} + dBm0_{h,v} + A_{gas} \quad (7)$$

The sun does not perfectly illuminate the antenna because the antenna is scanning and because the solar beam width is smaller than the one of the antenna and the ray width (typically 1°). An estimation of this averaging effect and the associated "apparent" attenuation of the solar signal is given in Holleman et al., 2008. There, they approximate the antenna pattern and the solar power with a Gaussian distribution. The fraction of solar power "seen" by the Radar system can be estimated as the area integral of the product of those two Gaussian distributions over the ray width of 1°. The solar beam width amounts to 0.54° whereas the beam widths of the horizontal and vertical beam are 0.95 and 0.94°, respectively. The transmission loss amounts to 0.68 dB, if there is perfect alignment of antenna and sun. An additional correction factor needs to be applied due to azimuthal scanning losses when the received solar signal is smeared over the ray width. For a ray width of 1° and a perfect alignment of the sun with the antenna the total loss P_L amounts to 1.56 dB.

P_L is the loss which accounts for the effects mentioned above, so that received power (in dBm) can be written as:

$$P_{h,v} = SNR_{h,v} + dBm0_{h,v} + A_{gas} + P_L \quad (8)$$

The received solar power as described above is however dependent on pulse width. Since we employ 0.4 μs and 0.8 μs pulse widths in the scan strategy we use SNR data to estimate the peak solar SNR, because SNR is independent of pulse width. The solar power is computed from range bins at a height $z > 12$ km in order to avoid artifacts (e.g. clutter, weather echoes). This is done individually for the two pulse widths.

4. Estimating antenna misalignment and the peak solar radar power using solar flux measurements

The method to determine antenna misalignment is described in Holleman and Beekhuis (2004). In reality, the main "beam" of the sun is sampled at antenna positions which do not match exactly the current position of the sun (beam width of the antenna is 1 degree versus 0.5 degree of the sun). That means depending on the position of the antenna and the sun, the antenna is more or less perfectly illuminated by the sun. The probability, that the solar beam perfectly illuminates the antenna is rather small based on extracted sun rays from the operational scanning mode. However, if we have a sufficient large sample of solar encounters we may fit a 2-d surface of a Gaussian type to the radar measured solar power in terms of the difference between the antenna position and the solar coordinates, i.e. $x_{H,V} = az_{radar} - az_{sun}, y_{H,V} = el_{radar} - el_{sun}$. The peak solar flux $P_{H,V,m}$ is determined from the fitted surface which then can be compared to the independent solar flux measurement. This analysis is carried out independently for both the horizontal and vertical channel and the peak solar power is determined from the fitted 2-d surface. Perfect antenna positioning is found for $x_{H,V,m} = 0$ and $y_{H,V,m} = 0$. A nonzero value of $x_{H,V,m}$ and $y_{H,V,m}$ quantifies the antenna positioning error. A difference between $x_{H,m}$ and $x_{V,m}$ and, similarly for y, is an indicator for an antenna mis-alignment of the feed in H and V. That would mean that the antenna may be less sensitive for a given polarization compared to the other polarization for a point target (sun). At a given range, the antenna would "see" different sample volumes at the respective polarization which may be of relevance in situation with large spatial reflectivity gradients. Since this analysis is carried out for both polarizations we can also quantify the differential sensitivity of both receiver channels. For a given day, we compute the misalign-

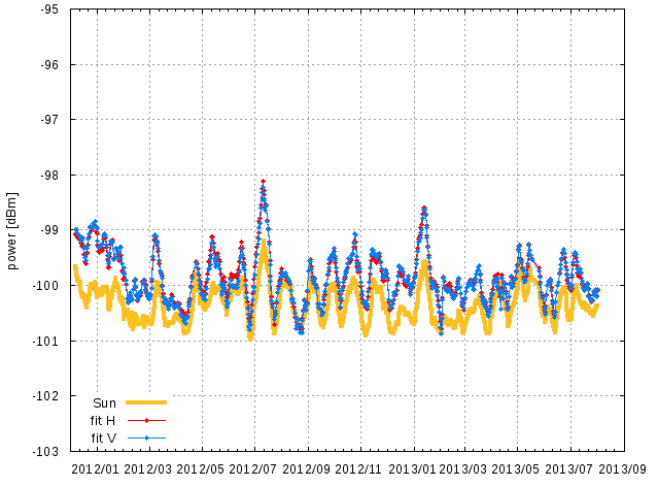

Figure 1: Long term (starting November 2011) solar power versus solar power from radar data, radar site Neuhaus.

ment using solar rays collected over the last three days. The peak solar power from operational radar data has been verified against dedicated measurements, where the radar is pointing directly into the sun. The agreement is better than 0.5 dB.

5. Results from the solar monitoring

As an example, the longterm comparison for the radar Neuhaus (NEU; starting November 2011) between sun and radar is shown in Figure 1. This graph shows how the solar power seen by the radar follows closely the independent solar power measurement. There has been no change in calibration and no adjustment of antenna pointing during this period.

Figure 2 shows the differential power H-V for both pulse widths, and difference between solar power and radar power in H and V, again for both pulse widths.

These figures give an impression on how the differences evolve as a function of time. Over the one-year period, the differential power is stable within $\pm$ 0.1 dB. The median power differences between sun and radar for nine radars are shown in Table 1. The overall statistics (average over nine sites) from November 2011 are

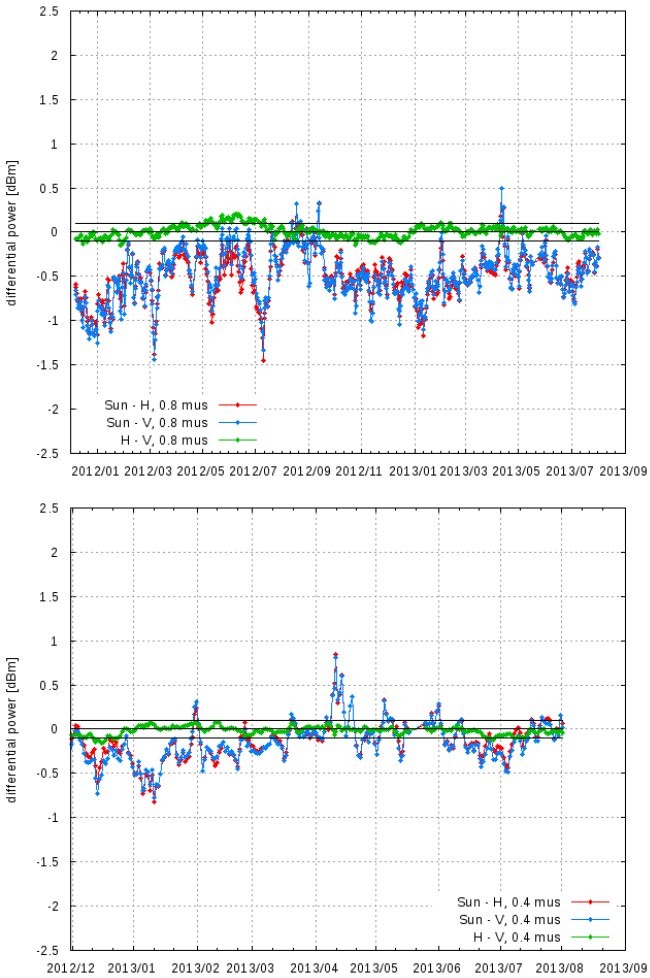

Figure 2: Differential power (sun - radar H,V) and H-V for 0.8 μs, upper panel, and for 0.4 μs, lower panel. The time series for 0.4 μs begins in December 2012 after the new scan strategy (which includes now a pulse width of 0.4 μs) has been introduced, the 0.8 μs data begins November 2011.

Table 1: Statistics of the difference between sun and radar sun data (in dB) averaged over all nine radar sites. Data are filtered for periods where system were not operational. The table shows data for pulse widths (PW) 0.4 and 0.8 μs. Here we consider data starting November 2011.

	PW 0.4 μs	PW 0.8 μs
1st Q H	-0.6	-0.9
med H	-0.3	-0.6
3rd Q H	-0.01	-0.3
1st Q V	-0.5	-0.6
med V	-0.2	-0.2
3rd Q V	+0.1	0.0

Table 2: Statistics of the difference between sun and solar radar data (in dB) averaged over all nine radar sites. Data are filtered for periods where system were not operational. The table shows data for pulse widths (PW) 0.4 and 0.8 μs. This is the performance since 14.3.2013.

	PW 0.4 μs	PW 0.8 μs
1st Q H	-0.3	-0.5
med H	-0.1	-0.3
3rd Q H	0.1	-0.2
1st Q V	-0.4	-0.5
med V	-0.1	-0.1
3rd Q V	+0.2	+0.1

given in Table 1 and the more recent values since March 2013 are shown in Table 2. The more recent data consider up-to-date calibrated radar systems. The results show that the receiver sensitivity is characterized well for both pulse widths and polarizations with a bias of $\approx -0.2 - -0.6$ dB for the whole time period considered. The more recent data shows an improvement, where the bias is around -0.1 dB.

We also use the Neuhaus site to demonstrate the stability of the pointing accuracy. The pointing accuracy in azimuth and elevation using solar radar data from the H and V receiver channel is shown in Figure 3. In general, the pointing accuracy for this ≈ 20 month period is within the target accuracy of $\pm 0.1^\circ$. The increase around 12.4.2013 (increase of az bias to 0.3°, also seen in the differential power, see e.g. Figure 2) is related to a software upgrade where accidently erroneous angle offsets were introduced into the radar configuration. This error was quickly detected and fixed because of the monitoring of solar radar signals. Note also the effect on the differential power where a bias up to 1 dB is found (Figure 2, lower panel). The beam squint computed from the positioning bias in H and V is shown in Figure 4 (see also Frech et al. 2013). The beam squint was specified to be smaller 0.06°, a value that it easily achieved by this antenna.

6. Monitoring the absolute calibration

The absolute calibration of the radar system maybe checked during the radar acceptance test using for example a metal sphere or other targets with a well defined radar cross section (see e.g. Atlas, 2002) for an overview on calibration methods). In practice those measurements are sometimes not feasible in the field, so that we often rely on a proper specification of the radar system by the radar manufacturer. Some important parameters such as antenna gain may have substantial uncertainty (on the order of 0.5 dB or more) when using a standard gain horn as a method to determine the antenna gain of a dualpol antenna. Other "constants" in the radar equation (losses) are usually measured once during an radar acceptance and often are assumed to be constant during the lifetime of a radar system. In that respect we are looking into methods which enable us to monitor the stability of the radar calibration during operation. The goal is to keep the bias in Z to be lower than ± 1 dB.

From literature we were aware that a wet radome may bias differential moments significantly, so we equipped a number of radar sites with optical disdrometers in order to monitor and quantify possible biases induced by a radome as a function of precipitation rate (Frech et al, 2011). Aside from this radome specific application, the Thies optical disdrometers (termed present weather sensor, PWS) appears to be a promising instrument to verify the absolute calibration as it provides a direct means to

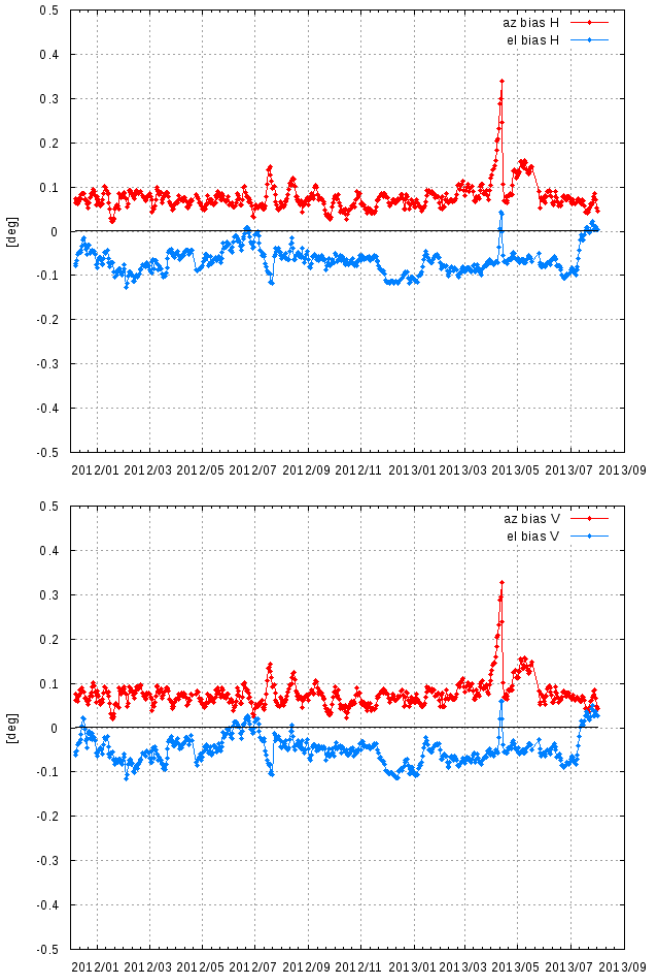

Figure 3: Long term (starting November 2011) antenna positioning bias in elevation and azimuth, radar site Neuhaus. Bias is determined using data from the H receiver channel (upper panel), and the receiver channel V (lower panel).

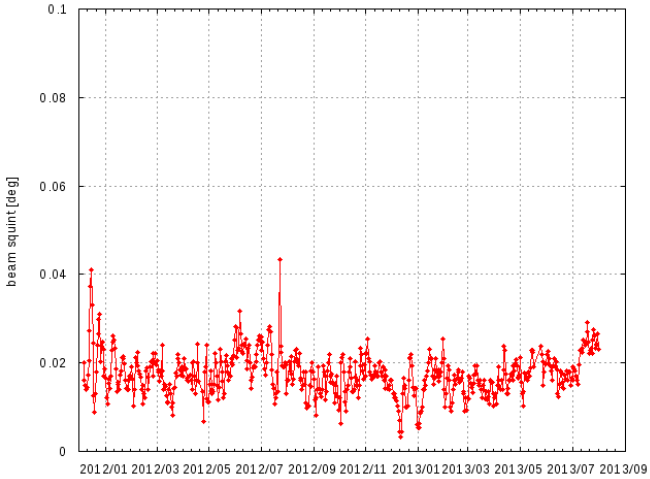

Figure 4: Long term (starting November 2011) beam squint data, i.e. the mismatch of the main lobe between H and V, radar site Neuhaus.

verify the radar reflectivity factor.

We briefly describe the measurement principle of the PWS. A laser light sheet is illuminating a sensing volume. If precipitation is falling through the sensing volume, the degree of attenuation relates to the particle size, and the length of the attenuated signal links to the fall speed of the particle. Precipitation type is determined by the drop size distribution and the observed fall speeds. Using parameterized falls speed relationships for hydrometeors, the radar reflectivity factors are computed as a standard output using the measured dsd. When relating this in-situ measurements with the radar measurement, we have to assume that the precipitation characteristics of the PWS are comparable to the ones observed by the radar sensing volume. Schematically the setup is illustrated in Fig 6. We evaluate the first range bin in the far-field of the birdbath scan, i.e. 650 m above the radar site. The assumption is that the drop size distribution (dsd) and hydrometeor type do not change significantly between this hight level and the surface, where the PWS is situated. We also require that the bright band is above the 650 m level.

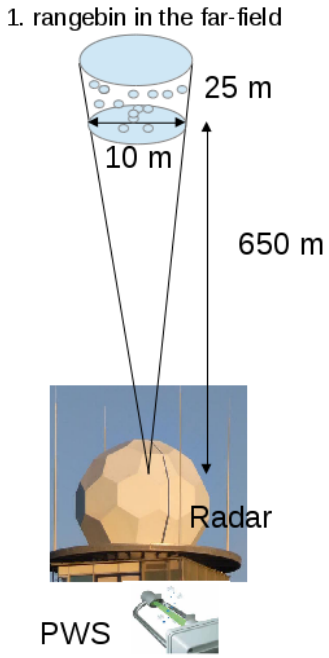

Figure 5: Schematic setup of the absolute calibration monitoring. A measurements of a PWS at the radar site is related to the first range bin radar volume 650 m above the radar site.

a. *Data acquisition*

As part of the operational scanning, a 90° elevation (birdbath) scan is performed every 5 minutes at the end of the volume scan. The main purpose of this scan is to monitor the offset of ZDR and Φ_{dp}. Two sweeps are performed with 0.4 μs and 0.8 μs pulse length, respectively.

The basic scan parameters are briefly summarized in the following:

- elevation: $90°$
- az speed: $48°/s$
- dynamic angle syncing (DAS): $5°$
- range sampling: 25 m, no range averaging
- PRF: 2400 / 1500 Hz
- pulse width: 0.4 and 0.8 μs
- range: 20 km

The scan is specified such that it can run in a very short time period. We therefore use the maximum antenna rotation speed. Since we do not need any azimuth resolution at this elevation we specify the largest possible DAS angle interval of $5°$ to sample as many pulses as possible within a ray. At a given range, radar moments are averaged over all azimuth angles. Thus canting effects on ZDR are averaged out.

The PWS is configured to provide data every minute. So we obtain the measured dsd, the computed radar reflectivity factor, a hydrometeor classification at a minute resolution.

b. *Data analysis and results*

When evaluating the radar data with the PWS data we make the following assumptions: The HM fall velocity has to be larger than 4 m/s and smaller than 8 m/s (Yuter et al, 2006), the PWS derived radar reflectivity factor Z has to be between 20 and 30 dBZ, $\rho_{hv} > 0.98$ and the temperature at 650 m must be $> 4°$. The radar Doppler velocity of the birdbath scan at 650 m is assumed to be the HM fall velocity. We assume a moist adiabatic temperature gradient to estimate the temperature at 650 m by using the PWS temperature measurement. Furthermore, a

radar measurement is related to a PWS sample with a $+2$ minute offset. In that case we make the assumption that the hydrometeors at 650 m with a fall speed of 5 m/s reach the surface in about 2 minutes. With those conditions we attempt to isolate measurements with rather stratiform rain conditions. As a sensitivity study for this analysis we filtered the PWS data to test the stability of the results as a function of the surface wind speed near the disdrometer. This is because disdrometers may have substantial errors under conditions with stronger winds. We find however that the results presented below remain stable so that we do not further discuss this here. This may suggest that the initial filter conditions implicitly eliminate problematic PWS data.

A typical time series example on how the radar data compares to the PWS data is shown Figure 6. It highlights some aspects of the filtering procedure. In this example there are periods where we find qualitatively a good agreement between the PWS and the radar data. There is a shower passing over the radar site at about 8 UTC on 10th November. Rain rates around 0.8 mm/h are measured, and the reflectivity factor is up to 25 dBZ. The difference between the PWS and radar Z is clustering around 0 dB with a spread of ± 5 dB. The corresponding HM fall velocities are near 5 m/s which is indicative for the presence of predominantly small rain drops (size 1-2 mm). ZDR is close to zero and ρ_{hv} is near 1. There is also a case around 8 UTC, 11th November where small rain rates are measured on site. This is a situation where we have a fog layer producing drizzle at the surface which is mostly not reaching up to 650 m. During this period smaller ρ_{hv} and the small fall velocities on the order of cm/s suggest particles in the ice-phase. These situations are filtered in the following, when we look at the statistics this data.

A one-to-one comparison of the PWS Z and the radar Zh and Zv is shown in Figure 7. On average we notice fairly good correspondence between the PWS and radar measurement even if we are not filtering the data. The H polarization appears to have a bias towards larger Z values compared to the PWS data. The MHP statistics for the filtered data (the red colored data in Figure 7) is summarized in Table 3). There we show the bias (defined as the median of the differences between PWS and radar samples) and first and third quartile. In addition we show the results from the solar monitoring where we

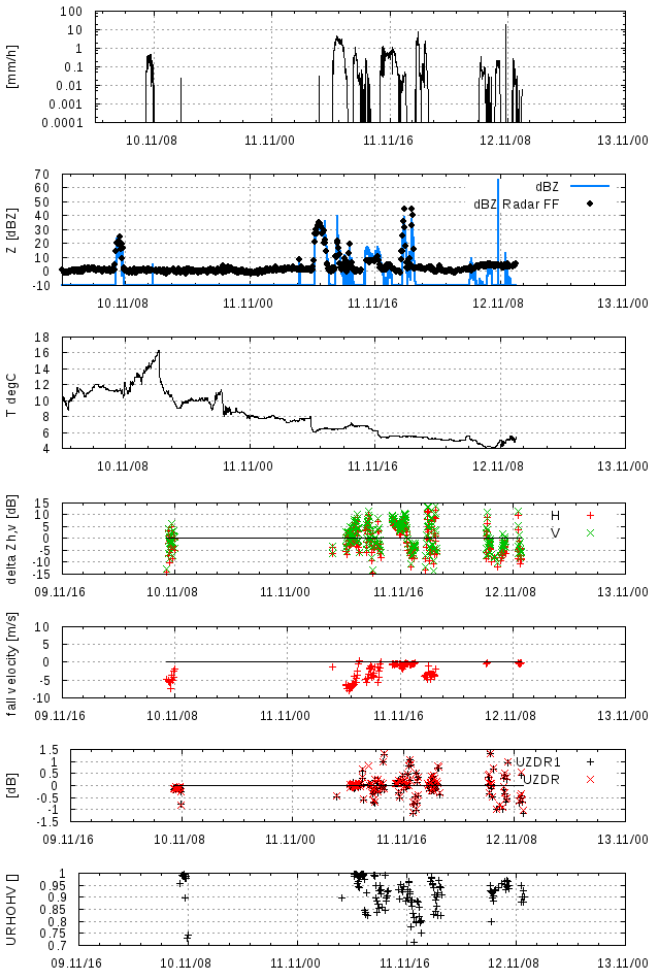

Figure 6: Time series of measured and computed quantities from the PWS and the radar, about a one day period taken in November 2012. The indicated time has the format dd.mm/hh. From the top to the bottom we have: the PWS precipitation rate [mm/h], the reflectivity factors from the PWS and first far-field range bin (dBZ; FF: far-field), the surface temperature [°C], the difference between PWS and radar reflectivity factor [dB] ($Z_{PWS} - Z_h$, $Z_{PWS} - Z_v$), the HM fall velocity [m/s], the differential reflectivity ZDR and ZDR1 (latter computed from the first lag autocorrelation function), and the cross correlation coefficient ρ_{hv}.

Table 3: MHP: Statistics (1st and 3rd quartiles and the median) of the filtered differences between PWS and radar far-field data for a 4 month data period. The data cover a time period from 6.7.2012 until 9.10.2012. In addition we show the corresponding statistics for the difference between sun and radar sun data (in dB). The table shows data for a 0.8 μs pulse width. $\Delta Z = Z_{PWS} - Z_{Radar}$, $\Delta P = sun - P_{sun,Radar}$.

	1st Q	Median	3rd Q
ΔZ_h	-3.2	-1.0	0.8
ΔZ_v	-1.8	0.3	2.2
ΔP_h	-1.7	-1.4	-1.2
ΔP_v	-0.5	-0.2	0.0

quantify the bias of the receiver sensitivity as the difference between solar power and the solar power seen by the radar for the same period. For MHP the results show a bias in Z of -1 dB in H and $+0.3$ dB in V. The corresponding bias of the receiver is -1.4 dB (H) and -0.2 dB (V). This suggests that the main contribution to the bias in the H channel has its origin in the receive path, because the bias comprising the transmit and receive path is actually smaller. In comparison to the H channel, the V channel shows small errors. Corresponding results for the BOO radar are shown in Table 4. We find a bias in Z of $+0.7$ and $+1.0$ dB, in H and V, respectively. The corresponding biases of the receiver based on the analysis of solar signals indicates a bias of -0.3 (H) and $+0.2$ dB (V). Contrary to the MHP results, a larger fraction of the bias appears related to the transmit path. This is true for both H and V.

We now show the status from three months starting 1.5.2013 until 1.8.2013, where data from the radars OFT, BOO and MHP are available. We focus on the median of the differences which is considered to represent the bias. The results are summarized in Table 5. For a direct comparison we also show the results from the previously discussed time period (in brackets). The biases of the OFT radar are within 1 dB. For MHP we find now a bias somewhat larger than 1 dB. Between the two periods (where the bias in Z_h changed from -1.0 to $+1.2$ dB) there was a re-calibration due to a transmitter modification which may explain the differences. The receiver bias is nearly

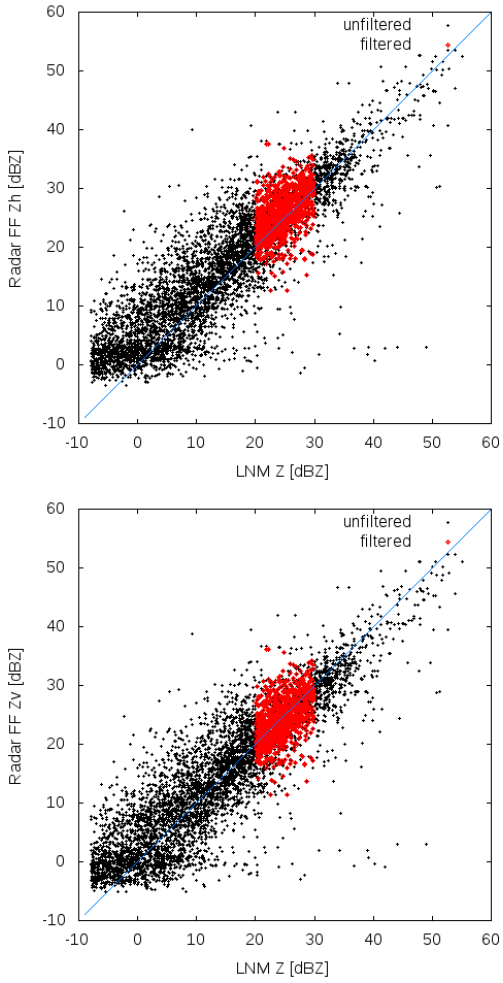

Figure 7: One-to-one comparison of radar reflectivity factors derived from the PWS and the radar far-field measurement, MHP data. Upper panel, Zh, the horizontal polarization, and lower panel Zv, the vertical polarization, at the far-field (FF) range. The data cover a time period from 6.7.2012 until 9.10.2012. Black dots represent all data measured during this period, and the red data are thresholded data: $20 < Z < 30$ dBZ; HM fall velocities between -4 and -8 m/s only, based on the radar Dopper data; temperature $> 4°$C at 650 m above the radar. Radar data shown are with a pulse width of 0.8 μs.

Table 4: BOO: Statistics (1st and 3rd quartiles and the median) of the filtered differences between PWS and radar FF data for a 4 month data period. The data cover a time period from 6.7.2012 until 9.10.2012. In addition we show the corresponding statistics for the difference between sun and radar sun data (in dB). The table shows data for a 0.8 μs pulse width.

	1st Q	Median	3rd Q
ΔZ_h	-1.0	0.7	2.4
ΔZ_v	-0.8	1.0	2.6
ΔP_h	-0.5	-0.3	-0.1
ΔP_v	0.0	0.2	0.4

Table 5: Radars MHP, OFT and BOO: mean bias (median) based on the filtered differences between PWS and radar FF data for a 3 month data period (in dB). The data cover a time period from 1.5.2013 until 4.8.2013. In addition we show the corresponding statistics for the difference between sun and radar sun data (in dB). The table shows data for a 0.8 μs pulse width. The figures in brackets are the results from the time period discussed previously (6.7.2012 until 9.10.2012)

	MHP	OFT	BOO
Median ΔZ_h	1.2 (-1.0)	0.0	1.7 (0.7)
MedianΔZ_v	1.1 (0.3)	-0.8	1.7 (1.0)
Median ΔP_h	0.1 (-1.4)	-0.5	-0.3 (-0.3)
Median ΔP_v	0.1 (-0.2)	0.3	-0.1 (0.2)

zero now. The bias in Z in BOO is now close to 2 dB whereas the receiver bias remains constant and close to zero. We also had a re-calibration and transmitter modification at this site. Further investigations with respect to the transmitter is still going on.

For completeness we show the one-to-one comparison of PWS and radar far-field data for the radar MHP in Figure 8. There is larger scatter now compared to Figure 7. More often we see large Z_{PWS} and small Z_{radar} values. This can be explained by more frequent events in this year's late spring where we had rain at the surface, and snow at the first far-field range bin (note that the MHP radar is 1000 m asl).

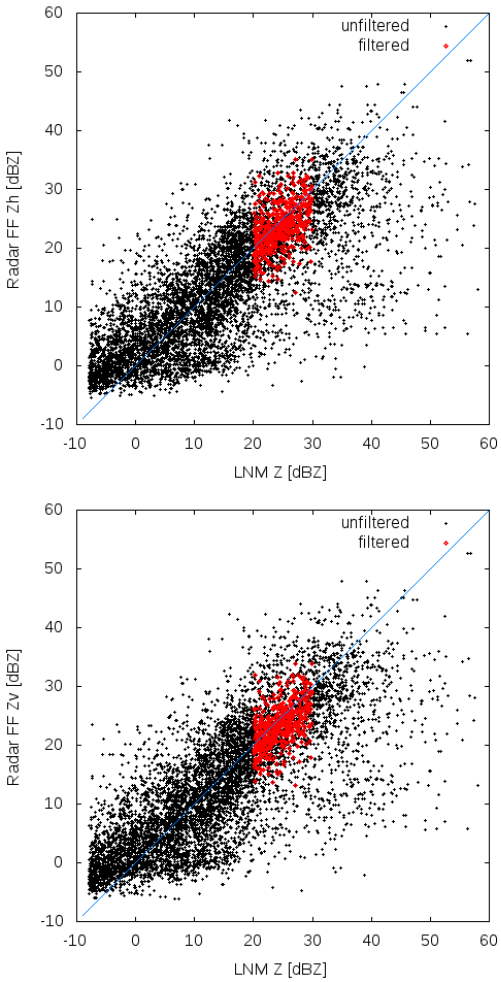

Figure 8: One-to-one comparison of radar reflectivity factors derived from the PWS and the radar far-field measurement, MHP data. Upper panel, Zh, the horizontal polarization, and lower panel Zv, the vertical polarization, at the far-field (FF) range. The data cover a time period from 1.5.2013 until 1.8.2013. Black dots represent all data measured during this period, and the red data are thresholded data: $20 < Z < 30$ dBZ; HM fall velocities between -4 and -8 m/s only, based on the radar Doppler data; temperature $> 4^{\circ}$C at 650 m above the radar. Radar data shown are for a pulse width of 0.8 μs.

c. *Discussion*

The previous results show that solar monitoring of the receiver path and the monitoring of the absolute calibration using a PWS helps to assess and identify calibration issues. The mean bias of the absolute calibration for the radar system OFT is better 1 dB. For the radar MHP, the bias is around $+1$ dB as compared to $+1.7$ dB for the system BOO. The small bias of the receiver sensitivity suggests that the bias in absolute calibration is related to the transmit path. This is a matter of ongoing investigation since there were modifications in the transmit path for those systems. However, with this combination of methods we are able to identify the potential source of error. The main advantage of this approach is the close proximity of the measurements such that uncertainties related to propagation effects and other sources of errors (i.e. sampling errors when relating measurements of a small to a large sampling volume; clutter effects) are minimized. The goal is now to equip all remaining systems with a PWS and to extend the methodology to snow situations.

7. Monitoring the ZDR and PhiDP offset

a. *ZDR offset*

The ZDR offset is currently a static offset which has to be set manually. It is part of a list of processing parameters needed by the signal processor to compute ZDR. There is currently only one offset for all pulse widths.

Commonly a birdbath scan is employed to assess the ZDR offset. The key assumption of the method is that ZDR is zero when looking at falling raindrops from below. Canting effects are averaged out by averaging ZDR data over azimuth. A deviation from zero is then attributed to a differential offset in the transmit and/or receive path. In addition we have to note, that the differential bias can be pulse width dependent, because of the traditional calibration approach currently in place (individual calibration of the H and V channel, separately for H and V). So in total, the pulse width dependent ZDR offset is determined by:

$$\Delta_{TX,RX} = \Delta_{RX} + \Delta_{TX} \quad (9)$$

The differential bias in of the RX path can be due to differential receiver gain in H & V and due to uncertainties of the measured losses. For the transmit path, a differential bias might be due to uncertainties of the losses (circulators, waveguide, splitter) and uncertainties in the antenna characterization (H & V antenna gain, width of the main lobe). In addition, temperature effects may also contribute to a differential offset. We have found that the radome temperature has to be kept within a 5 K interval in order to have the temperature dependent ZDR bias lower than 0.1 dB for a temperature range between 0 and 15°C. For higher temperatures it appears that the ZDR bias has only a weak temperature sensitivity (see below).

In order to quantify the differential offset in the receive path, Δ_{RX}, solar signals can be analyzed. Since the sun is an unpolarized source of radiation, the solar differential reflectivity should be zero. However, differences in receive path may result in an systematic hardware specific offset. The differential reflectivity may be computed directly from the sun ray data without correcting for the fact that the sun is usually not perfectly hit by an individual ray. We compute a range averaged median ZDR for each ray, only for range bins that are 12 km above the surface avoiding for example clutter effects). A median ZDR is then computed from all rays for a given day.

A median ZDR from the birdbath scan is computed when there is precipitation at a given day. The starting point is the birdbath scan at a given time. We first compute a range averaged ZDR for a given ray, starting in the far-field. We require that $\rho_{hv} > 0.9$ and SQI > 0.5, and that there are at least ten valid range bins. We then compute the median ZDR from all rays of the sweep. In order to obtain the diurnal averaged ZDR, the median ZDR from all birdbath scans of a given day is computed. We compute only an average if there are at least 6 birdbath scans available with valid data. We also store the 1st and 3rd quartile. We do not further separate out the precipitation type.

As an example we show data from the radar NEU for the 0.4 and 0.8 μs pulse widths (Figure 9). The data cover a period of 9 months, including winter and summer. First of all, ZDR based on the birdbath scan is constant within 0.1 dB for both pulse widths. There is a somewhat larger variation for the solar ZDR, but still the variation is within 0.1 dB. During this period only one offset adjust-

ment has been applied. Here we have a relatively good match of ZDR from 0.4 and 0.8 μs pulse widths (difference is < 0.1 dB).

The actual ZDR offset Δ_{TX,RX,t_i} based on the latest birdbath scan is also shown in Figure 9 (red curve). Ideally this value should closely match the constant offset of the system.

If the offset $\Delta_{TX,RX}$ is properly set initially at a given time t_0, we have

$$0 \quad = \quad ZDR_{90^\circ,t_0} - \Delta_{TX,RX,t_0} \tag{10}$$

Δ_{TX,RX,t_0} is the static offset which is stored as an initial parameter in the signal processor.

Now, if we find at a given time t_i

$$0 \quad \neq \quad ZDR_{90^\circ,t_i} - \Delta_{TX,RX,t_0} \tag{11}$$

the offset needs to be adjusted. The nonzero ZDR offset is now

$$ZDR_{TX,RX,t_i} \quad = \quad ZDR_{90^\circ,t_i} - \Delta_{TX,RX,t_0} \tag{12}$$

In order to compute a zero ZDR, the offset is corrected. The new system offset Δ_{TX,RX,t_i} is then

$$\Delta_{TX,RX,t_i} \quad = \quad \Delta_{TX,RX,t_0} + ZDR_{TX,RX,t_i} \tag{13}$$

If this value starts to deviate too much ZDR data can be corrected automatically in a post-processing step, before the offset is adjusted remotely by service personnel. Aside from transition times (where the offset has been adjusted manually; this will be fixed in the future) the actual offset Δ_{TX,RX,t_i} matches the system offset with 0.1 dB for the NEU system (Figure 9).

The increased variation in ZDR due to temperature variations in the radome and subsequently in the receiver is shown in Figure 11. The upper panel shows data from the radar MHP and the lower panel from the radar NEU. Due to an issue with the air conditioning, the temperature variations at MHP are much larger than in NEU. In the first half year, where we frequently have temperatures down to 10°C, we find variation in ZDR on the order of 0.2 dB. This is also found for the ZDR derived from solar data. With predominantly higher temperatures in the last 3 months (where we do not expect a significant temperature dependency of ZDR), the variability in ZDR is

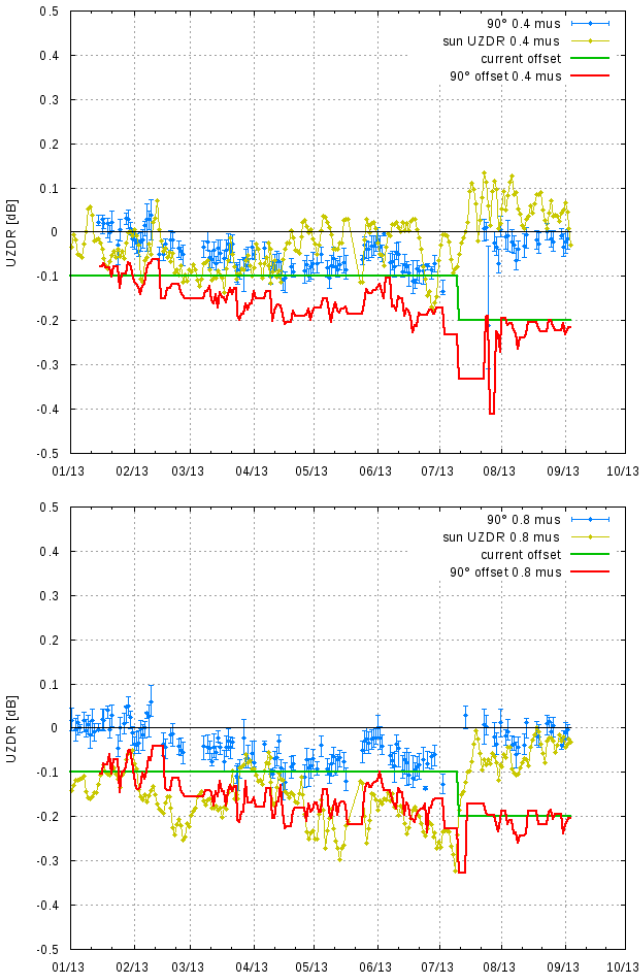

Figure 9: Monitoring the differential offset of ZDR, radar Neuhaus, NEU. The upper panel shows the result for a 0.4 μs pulse width, and the lower panel for a 0.8 μs pulse width. The blue data represent diurnal averaged ZDR data (when precipitation is present). UZDR denotes differential reflectivities that are computed from unfiltered data. "sun UZDR 0.4 μs": differential reflectivity based solar data; "current offset": system ZDR offset; "90° offset 0.4 μs": this is the offset that should be applied based on the latest ZDR values derived from the birdbath scan.

much smaller. This is highlighted further if we compare the MHP data with NEU data. In NEU temperatures are kept at a higher level and the temperature range is small ($<$ 5 K). For the whole period, ZDR is essentially constant.

If we keep the temperatures in a fairly narrow range (Neuhaus example), the differential reflectivity is very stable. There is certainly no day-to-day adjustment of this parameter necessary. Longer precipitation free periods are not an issue (sometimes addressed as a problem using the birdbath scan to monitor ZDR offset). Aside from this, solar derived ZDR is able detect issues in receiver path as the data are available on a daily basis. Note also, that based on this result, a detailed classification of the HM type is not necessary to monitor the ZDR offset. The data in Figure 11 cover winter and summer weather.

b. *PhiDP offset*

The birdbath scan is also used to determine and monitor the Φ_{dp} offset. Typically the waveguide length for the H and V pulse is different, so that there is a hardware specific offset which will be different but constant from site to site. The reference offset for Φ_{dp} can be any number, here we determine the offset so that the resulting Φ_{dp} is close to zero degree. Monitoring Φ_{dp} can help to detect problems for example with the wave guide (e.g. a mechanical failure). The computation of the mean Φ_{dp} follows that of ZDR. The difference is that only range bins are considered where we have $Z_h > 20$ dBZ and $\rho_{hv} > 0.98$. Similar to the ZDR time series we find less scatter in Φ_{dp} from day to day ($< 1°$) . Larger variations are found at the MHP site (up to $3°$). Again, we relate this to a temperature sensitivity of this parameter. Negative values seen in the MHP data are related to software configuration tests.

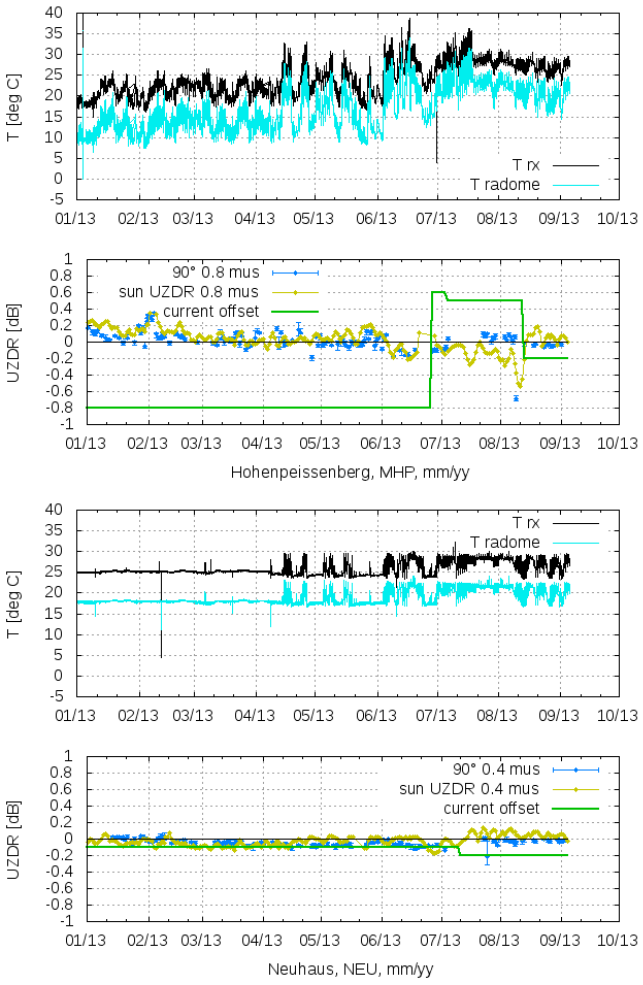

Figure 10: Temperature sensitivity of ZDR, upper panel radar Hohenpeissenberg, MHP, and lower panel radar Neuhaus, NEU. Shown are time series that start 1.1.2013.

8. Summary

In this contribution we give an overview on the current status of the radar data quality monitoring within the new DWD polarimetric radar network. Currently nine systems are in operation and by the end of 2014 it is expected that the replacement of all 17 system will be finished. The

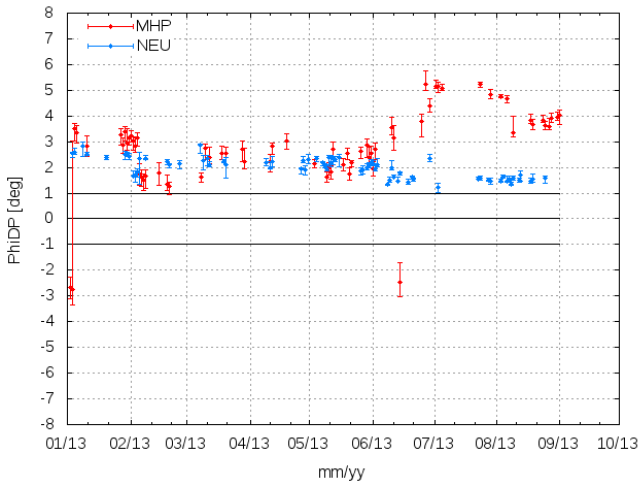

Figure 11: Mean Φ_{dp} determined from the birdbath scan. Neuhaus (NEU) and Hohenpeissenberg (MHP) data are compared.

radar data quality monitoring described here is one element of the new radar processing suite "POLARA" which is currently in an operational test phase. The following elements are currently covered by the data quality monitoring:

- receiver sensitivity,
- differential receiver sensitivity,
- antenna positioning and beam squint,
- absolute calibration,
- ZDR and Φ_{dp} offsets.

The receiver sensitivity and the differential sensitivity (difference of the H and V channel) are analyzed using solar interference data. The statistics over a 22 month period for the radar Neuhaus shows that the overall magnitude of the bias (determined relative to an independent sun power measurement) is smaller than 0.6 dB. The more recent data shows a reduction of the bias to values below 0.3 dB. The differential power is constant to within ± 0.1 dB. This magnitude of bias is also found on all other systems.

Radar positioning accuracy is monitored by the analysis of solar interference data. This is done for both the H and V channels. From this the beam squint of the antenna is computed. We show that this method produces very stable results, variations are smaller 0.1° in Neuhaus. We also show that configuration errors (in this case a wrong elevation offset) can be quickly detected.

We use an optical disdrometer (PWS) to monitor the absolute calibration. Currently three sites are equipped with such a sensor. It provides a reference reflectivity factor Z computed from the measured drop size distribution. This Z is compared to the first far-field Z measured by a birdbath scan under stratiform rain conditions. The advantage of this setup is the close proximity of the reference instrument to the radar measurement. The method is embedded in the operational scanning so that it can provide a continuous picture on the absolute calibration quality.

We show the bias of Zh and Zv for three systems, pulse width 0.8 μs. The absolute bias ranges from 0.0 (perfect) to 1.7 dB. The latter value is found for the system in Boostedt where a number of transmitter tests and modifications were carried out . Further investigations on this are currently underway. Initially this system had a much smaller bias. Overall the results are very promising so that we plan to equip all sites with a PWS.

The birdbath scan and solar interference data are used to monitor and determine the ZDR offset. The signal processor is initialized with this static ZDR offset. The birdbath scan is operationally available every 5 min. For the Neuhaus radar we show that ZDR is constant within 0.1 dB for a 9 month period. This is shown for the pulse widths used in the operational scanning and the result includes summer and winter weather. Somewhat larger variation are seen in the solar ZDR, but variations are comparable to the birdbath data. Based on the actual birdbath scan we compute the deviation of the static of ZDR offset. If the actual offset deviates significantly, the offset can be adjusted or ZDR can be corrected in a post-processing step.

The temperature sensitivity of ZDR is shown comparing Hohenpeissenberg with Neuhaus data. Due to larger temperature variations in the Hohenpeissenberg system, variations in ZDR can be larger than 0.2 dB. In Neuhaus, where the temperature range is kept below 5 K, ZDR variations are much smaller. If the systems are oper-

ated in a temperature range smaller than 5 K, no day-to-day or even scan-to-scan adjustment of the ZDR offset is necessary. The results indicate that there is no drawback in having only infrequent precipitation, depending on the synoptic situation or season. As a backup, we have the measurements of solar ZDR which helps to identify possible issues in the receive path. This data are continuously available. Aside from the analysis of radar data, an extensive evaluation of the BITE is implemented on each radar site, which helps to detect degrading hardware components that may have an influence on the ZDR offset (not discussed here).

The birdbath scan is also used to determine the Φ_{dp} offset. Similar to the ZDR offset, the Φ_{dp} offset is very stable. We also find a temperature sensitivity of this moment.

As a next step, the method of monitoring the absolute calibration needs to be extended so that it can be used all year procedure (i.e. to be applied in mixed phase situations). It will be tested to adjust the calibration based on the PWS - radar comparison.

Acknowledgments: This work has been carried out within DWD's project "Radarmassnahmen". The discussions with Jörg Seltmann, Theo Mammen and Bertram Lange are greatly acknowledged.

References

Atlas, D.: 2002, Radar calibration: some simple approaches. *Bull. Amer. Meteorol. Soc.*, **83**, 1313–1316.

Figueras i Ventura, J., A.-A. Boumahmoud, B. Fradon, P. Dupuy, and P. Tabary: 2012, Long-term monitoring of French polarimetric radar data quality and evaluation of several polarimetric quantitative precipitation estimators in ideal conditions for operational implementation at C-band. *Quart. J. Roy. Meteorol. Soc.*, **138**, 2212–2228.

Frech, M.: 2009, The effect of a wet radome on dualpol data quality. *34rd AMS Conf. on Radar Meteorology, Williamsburg, VA*, AMS, 7p.

Frech, M., B. Lange, T. Mammen, J. Seltmann, C. Morehead, and J. Rowan: 2013, Influence of a radome on antenna performance. *J. Atmos. and Oceanic Tech.*, **30**, 313–324.

Holleman, I. and H. Beekhuis: 2004, Weather radar monitoring using the sun. Technical report, KNMI TR-272.

Holleman, I., A. Huuskonen, M. Kurri, and H. Beekhuis: 2010, Operational monitoring of weather radar receiving chain using the sun. *J. Atmos. Ocean. Tech.,*, **27**, 159–166.

Huuskonen, A. and I. Holleman: 2007, Determining weather radar antenna pointing using signals detected from the sun at low elevations. *J. Atmos. Ocean. Tech.*, **24**, 476–483.

Melnikov, V. M.: 2004, Simultaneous transmission mode for the polarimetric WSR-88D: Statistical biases and standard deviations of polarimetric variables. Technical report, NOAA/NSSL, Norman Oklahoma.

Saemundsson, T.: 1986, Atmospheric refraction. *Sky and Telescope*, **72**, p70.

Seltmann, J. E. E., T. Hohmann, and M. Frech: 2013, DWD's new operational scan strategy. *36rd AMS Conf. on Radar Meteorology, Breckenridge, CO*, AMS.

Steinert, J., M. Werner, and P. Tracksdorf: 2013, Hydrometeor classification and quantitative precipitation estimation from quality assured radar data for the DWD polarimetric C-band weather radar network. *36rd AMS Conf. on Radar Meteorology, Breckenridge, CO*, AMS.

Tapping, K.: 2001, Antenna calibration using the 10.7 cm solar flux. *Workshop on Radar Calibration, Albuquerque, NM*, AMS.

Tracksdorf, P., N. Rathmann, M. Werner, J. Steinert, and M. Frech: 2013, Operational utilisation of polarimetric C-band weather radar measurements at Deutscher Wetterdienst: The project "Radarmassnahmen". *36rd AMS Conf. on Radar Meteorology, Breckenridge, CO*, AMS.

Yuter, S. E., D. E. Kingsmill, L. B. Nance, and M. Löffler-Mang: 2006, Observations of precipitation size and fall speed characteristics within coexisting rain and wet snow. *J. Appl. Meteor. Clim.*, **45**, 1450–1464.